Inorganic Chemistry

Article

Forum

Crystal Structure of the Oxygen-Evolving Complex of Photosystem II

James Barber*

*Division of Molecular Biosciences, Faculty of Natural Sciences, Imperial College London,
London SW7 2AZ, U.K.*

The oxygen in our atmosphere is derived from and maintained by the water-splitting process of photosynthesis. The enzyme that facilitates this reaction and therefore underpins virtually all life on our planet is known as photosystem II (PSII). It is a multisubunit enzyme embedded in the lipid environment of the thylakoid membranes of plants, algae, and cyanobacteria. Powered by light, PSII catalyzes the chemically and thermodynamically demanding reaction of water splitting. In so doing, it releases molecular oxygen into the atmosphere and provides the reducing equivalents required for the conversion of carbon dioxide into the organic molecules of life. Recently, a fully refined structure of an isolated 700 kDa cyanobacterial dimeric PSII complex was elucidated by X-ray crystallography, which gave organizational and structural details of the 19 subunits (16 intrinsic and 3 extrinsic) that make up each monomer and provided information about the position and protein environments of the many different cofactors it binds. The water-splitting site was revealed as a cluster of four Mn ions and a Ca ion surrounded by amino acid side chains, of which six or seven form direct ligands to the metals. The metal cluster was originally modeled as a cubane-like structure composed of three Mn ions and the Ca^{2+} linked by oxo bonds and the fourth Mn attached to the cubane via one of its O atoms. New data from X-ray diffraction and X-ray spectroscopy suggest some alternative arrangements. Nevertheless, all of the models are sufficiently similar to provide a basis for discussing the chemistry by which PSII splits water and makes oxygen.

1. Introduction

Photosystem II (PSII) is a multisubunit complex embedded in the thylakoid membranes of plants, algae, and cyanobacteria.[1,2] This photosynthetic enzyme catalyzes the most thermodynamically demanding reaction in biology, namely, the splitting of water into dioxygen and reducing equivalents. The reaction is driven by solar energy and underpins the survival of essentially all life on our planet. It supplies the oxygen we breathe, it maintains the ozone layer needed to protect us from UV radiation, and, of course, it provides the reducing equivalents necessary to fix carbon dioxide to organic molecules that create biomass, food, and fuel. For these reasons, it is truly the "engine of life" and its

appearance about 2.5 billion years ago represented the "big bang" of evolution. An essential prerequisite for understanding and possibly mimicking the water-splitting reaction of PSII is the elucidation of the three-dimensional (3D) structure of the participating macromolecular subunits, including those directly involved in the water-splitting reaction. Indeed, unraveling the mechanism of this reaction within a structural framework is today one of the greatest challenges in photosynthesis research and science in general because, in contrast to chemical and electrochemical water splitting, which are thermodynamically highly demanding, the PSII-catalyzed biological water-splitting mechanism is truly remarkable, proceeding with very little driving force and moderate activation energies.

Here I review how X-ray crystallography is contributing to the goal of obtaining a full description of the molecular processes by which PSII functions as a light-driven producer of molecular oxygen.

* E-mail: j.barber@imperial.ac.uk.
(1) Barber, J. *Q. Rev. Biophys.* **2003**, *36*, 71–89.
(2) Satoh, K.; Wydrzynski, T. J.; Govindjee. In *Photosystem II. The light driven water: plastoquinone oxidoreductase*; Satoh, K., Wydrzynski, T. J., Eds.; Springer: Dordrecht, The Netherlands, 2005; pp 11−22.
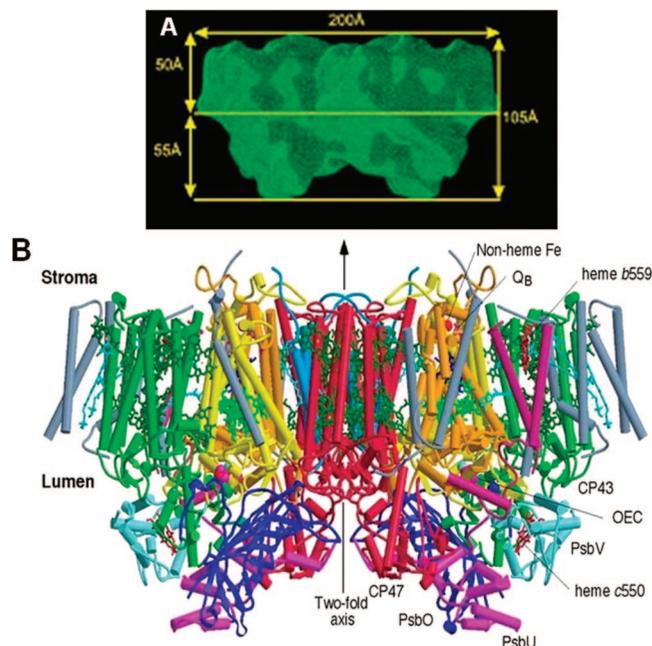
Figure 1. Side view of the PSII dimer isolated from *T. elongatus* viewed perpendicular to the membrane normal derived from (a) electron cryomicroscopy and single-particle analysis in the absence of negative staining at a resolution of about 20 Å (Duncan, J.; Nield, J.; Barber, J., unpublished) and (b) X-ray crystallography at a resolution of 3.5 Å.[7] For the X-ray structure, helices are represented as cylinders with D1 in yellow, D2 in orange, CP47 in red, CP43 in green, Cyt b559 in wine red, PsbL, PsbM, and PsbT in medium blue, and PsbH, PsbI, PsbJ, PsbK, PsbX, PsbZ, and Ycf12 in gray.[22] The extrinsic proteins are PsbO in blue, PsbU in magenta, and PsbV in cyan. Chlorophylls of the D1/D2 RC are light green, Pheo's are blue, chlorophylls of the antenna complexes are dark green, β-carotenes are in orange, hemes are in red, nonheme Fe is red, and Q_A and Q_B are magenta. The oxygen-evolving centers (OEC) where water-splitting catalysis occurs is shown in red (O atoms), magenta (Mn ions), and cyan (Ca^{2+}) balls.

2. Charge Separation and Electron Transfer in PSII

Prior to recent structural work, a range of biochemical and biophysical techniques had provided a good understanding of the events that give rise to the primary and secondary electron-transfer processes leading to water oxidation (reviewed in refs 2 and 3). These processes are initiated by the absorption of light energy by the many chlorophyll and other pigment molecules associated with PSII. The nature of these PSII light-harvesting antenna systems varies under different growth conditions and with different types of organisms. However, within the PSII core complex, only chlorophyll a (Chl a) and β-carotene are found, bound mainly to the CP43 and CP47 proteins (see Figure 1). In total, there are about 36 Chl a and 11 β-carotene molecules per PSII core based on biochemical[4] and structural analyses.[5–8] (In fact, in the

case of the unusual cyanobacterium *Acaryochloris marina*, Chl a is replaced almost entirely by Chl d.[88])

The excitation energy absorbed by these pigments is transferred to the reaction center (RC) composed of the D1 and D2 proteins. Together these RC proteins bind all of the redox-active cofactors involved in the energy conversion process, and the following sequence of reactions occurs. A special form of Chl a, P, acts as an exciton trap and is converted to a strong reducing agent after excitation (P*). P* reduces a pheophytin molecule (Pheo) within a few picoseconds to form the radical pair state $P^{\bullet+}Pheo^{\bullet-}$. Within a few hundred picoseconds, $Phe^{\bullet-}$ reduces a firmly bound plastoquinone (PQ) molecule protein (Q_A) to produce $P^{\bullet+}PheoQ_A^-$. $P^{\bullet+}$, which has a very high redox potential (>1 V), oxidizes a tyrosine residue (Tyr_Z) to form $Tyr_Z^{\bullet}PPheoQ_A^-$ on a nanosecond time scale. The neutral tyrosine radical ($Tyr_Z^{\bullet}$) is formed because a deprotonation of its phenolic group is concomitant with its oxidation by $P^{\bullet+}$. In the millisecond time domain, Q_A^- reduces a second PQ (Q_B) to form $Tyr_Z^{\bullet}PPheoQ_AQ_B^-$. At about the same time, $Tyr_Z^{\bullet}$ extracts an electron from a cluster of four Mn atoms that bind the two substrate water molecules. A second photochemical turnover reduces Q_B^- to Q_B^{2-}, which is then protonated to plastoquinol and released from PSII into the lipid bilayer, subsequently oxidized by photosystem I (PSI) via the cytochrome b_6f complex. Two further photochemical turnovers provide a cluster of four Mn ions and a Ca ion (Mn_4Ca) with a total of four oxidizing equivalents, which are used to oxidize two water molecules to dioxygen. Each oxidation state generated in the oxygen-evolving complex (OEC) is represented as an intermediate of the S-state cycle,[9,10] of which there are five (S_0–S_4). In addition to these reactions, side reactions can occur under some conditions including the oxidation of a high potential cytochrome bound within the PSII core complex (Cyt b559), a β-carotene molecule, and a Chl a molecule (Chl_Z)[11–13] (see Figure 2). These side reactions occur on the tens of millisecond time scale and therefore do not compete with the electron-transfer pathway leading to water oxidation. Indeed, they probably only occur when the rate of water oxidation becomes limited and thus provide a protective mechanism against the detrimental reactions resulting from the very high redox potential of the long-lived P radical cation.[11–14]

3. Crystal Structures

3.1. Protein Subunits. The first crystal structure of PSII isolated from *Thermosynechococcus elongatus* was reported by Zouni et al.[5] Their structure was limited to a resolution of 3.8 Å, and the C_α backbones of many of the subunits were not fully traced. Although no side-chain positioning

(3) Diner, B. A.; Babcock, G. T. In *Oxygenic Photosynthesis. The Light Reactions*; Ort, D. R., Yocum, C. F., Eds.; Kluwer Academic Publications: Dordrecht, The Netherlands, 1996; pp 213–247.
(4) Barbato, R.; Race, H. L.; Friso, G.; Barber, J. *FEBS Lett.* **1991**, *286*, 86–90.
(5) Zouni, A.; Witt, H. T.; Kern, J.; Fromme, P.; Krauss, N.; Saenger, W.; Orth, P. *Nature* **2001**, *409*, 739–743.
(6) Kamiya, N.; Shen, J. R. *Proc. Natl. Acad. Sci. U.S.A.* **2003**, *100*, 98–103.
(7) Ferreira, K. N.; Iverson, T. M.; Maghlaoui, K.; Barber, J.; Iwata, S. *Science* **2004**, *303*, 1831–1838.
(8) Loll, B.; Kern, J.; Saenger, W.; Zouni, A.; Biesiadka, J. *Nature* **2005**, *438*, 1040–1044.

(9) Joliot, P.; Barbieri, G.; Chabaud, R. *Photochem. Photobiol.* **1969**, *10*, 309–329.
(10) Kok, B.; Forbush, B.; McGloin, M. *Photochem. Photobiol.* **1970**, *11*, 457–475.
(11) Tracewell, C. A.; Brudvig, G. W. *Biochemistry* **2003**, *42*, 9127–9136.
(12) Faller, P.; Pascal, A.; Rutherford, A. W. *Biochemistry* **2001**, *40*, 6431–6440.
(13) Telfer, A. *Philos. Trans. R. Soc. London* **2002**, *B357*, 1431–1440.
(14) Stewart, D. H.; Brudvig, G. W. *Biochim. Biophys. Acta* **1998**, *1367*, 63–87.
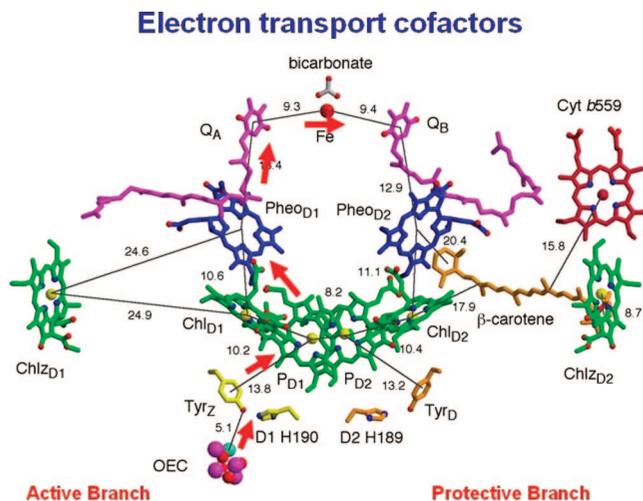
Electron transport cofactors

Figure 2. Cofactors involved in electron-transfer visualized perpendicular to the internal pseudo-two-fold axis.[7] The coloring scheme is the same as that in Figure 1. The phytyl tails of the chlorophylls and Pheos have been removed for clarity. The side chains of Tyr_Z (D1 Tyr161) and D1 His190 are shown in yellow and those of Y_D (D2 Tyr160) and D2 His189 in orange. The four chlorophylls comprising P680 are in direct van der Waals contact. The electron-transfer pathway is indicated by red arrows, and distances are given in angstroms. Excitation of the RC, via light absorption by chlorophylls (Chl) in the antenna, drives electron transfer from the cluster of four chlorophylls bound to the D1 and D2 proteins to the Pheo acceptor, leading to the radical pair $P680^{\bullet+}Pheo^{\bullet-}$. The radical cation of P is localized on P_{D1}, although the primary electron charge separation probably occurs from Chl_{D1} followed by hole migration,[29–31] while the radical anion is located on $Pheo_{D1}$. The electron on $Pheo_{D1}^{\bullet-}$ is rapidly donated to a firmly bound PQ Q_A (shown in purple) and then transferred to a second PQ Q_B (also shown in purple). This electron transfer is aided by the presence of a nonheme Fe located midway between them. When the PQ Q_B is fully reduced and protonated to plastoquinol (PQH_2), it diffuses from the Q_B binding site into the lipid matrix of the membrane. On the electron donor side, $P680^{\bullet+}$ is reduced by a redox-active tyrosine (Tyr_Z), which then extracts electrons from the Mn_4CaO_4 cluster that constitutes the oxygen-evolving center (OEC). These electron-transfer processes occur mainly on the D1 side of the RC, and the symmetrically related cofactors located on the D2 side (Chl_{D2} and $Pheo_{D2}$) are nonfunctional in primary charge separation. Other cofactors shown, including the heme of cytochrome b559 (Cyt b559 shown in red) and the β-carotene molecule (shown in brown), play a role in protecting PSII against photoinduced damage.[11–14]

was deduced, their model confirmed the dimeric organization of the isolated complex and the relative positioning of the major subunits and their transmembrane helices within each monomer derived from electron crystallography.[15–18] It also provided information on the positioning of cofactors involved in excitation transfer and charge separation. Most importantly, the analysis of the diffraction data provided the first direct structural hints of the Mn cluster of the OEC. Two years later Kamiya and Shen[6] reported a 3.7 Å crystal structure of PSII isolated from the *Thermosynechococcus vulcanus*, a cyanobacterium closely related to *T. elongatus*, and provided additional information to that revealed by Zouni et al.[5] The tracing of the main chains was more complete, and there was some effort made to assign amino acids, particularly those of the D1 and D2 proteins, as well as some

regions of the chlorophyll-binding proteins CP43 and CP47. Kamiya and Shen also assigned density for two closely located carotenoid molecules on the D2 side of the RC. Importantly, Kamiya and Shen's map contained electron density connecting to that attributed to the Mn cluster, which could be tentatively assigned to side chains of the D1 protein, including Ala344, Asp170, and Glu333 (or His332). Mutagenesis studies had already suggested that these residues could be ligands for the Mn ions,[19–21] and the X-ray-diffraction-derived model confirmed the concept that the C terminus of the D1 protein was intimately associated with the Mn cluster.[19] Kamiya and Shen[6] also suggested that, based on a weak electron density, D1 His337, D1 Asp189 (or D1 His190), and D1 Tyr73 may also be coordinated to Mn ions of the cluster.

As in the case of the earlier crystal structure,[5] the model of Kamiya and Shen did not include a Ca^{2+} bound close to the Mn cluster. Moreover, their model was only partially refined, and therefore many important questions were left unanswered. This changed with the publication of the Ferreira et al. crystal structure of PSII isolated from *T. elongatus* refined to a resolution of 3.5 Å.[7]

The side view of the PSII RC dimeric core complex of *T. elongatus* shown in Figure 1 is taken from the crystal structure of Ferreira et al.[7] and compared with an earlier low-resolution 3D structure determined by cryoEM and single-particle analysis on the same isolated complex (Duncan, J.; Nield, J.; Barber, J., unpublished). The PSII dimer has dimensions of 105 Å depth (of which 45 Å spans the membrane), 205 Å length, and 110 Å width and has a calculated total molecular mass of about 700 kDa.

The crystal structure was at sufficient resolution (3.5 Å) and refinement to assign virtually all of the amino acids that it contains. Overall, each monomer was found to consist of 19 different protein subunits where 16 are intrinsic and 3 extrinsic. There were in total 35 transmembrane helices per monomer depicted as cylinders in Figure 1. Details of the 19 different subunits assigned are given in Table 1, with one, Ycf12 (originally suggested to be possibly PsbN), being included based on more recent biochemical analysis of PSII.[22] The three extrinsic proteins PsbO, PsbU, and PsbV form a cap over the catalytic site where oxygen evolution occurs, preventing access by reductants other than water, while some of the low-molecular-weight subunits are located on the peripheral of the CP43/D1/D2/CP47 cluster, where they probably help to stabilize the binding of Chl and β-carotene molecules contained within the complex. The exceptions to this are the PsbE and PsbF proteins, which provide histidine ligands for the heme of Cyt b559, and the PsbL, PsbM, and PsbT proteins located at the monomer–monomer interface, where they possibly play a role in stabilizing the dimeric nature of the PSII complex. All of the small subunits have a single transmembrane helix except for PsbZ, which has two (see Table 1).

(15) Rhee, K.-H.; Morris, E. P.; Barber, J.; Kühlbrandt, W. *Nature* **1998**, *396*, 283–286.
(16) Hankamer, B.; Morris, E. P.; Barber, J. *Nat. Struct. Biol.* **1999**, *6*, 560–564.
(17) Hankamer, B.; Morris, E. P.; Nield, J.; Gerle, C.; Barber, J. *J. Struct. Biol.* **2001**, *135*, 262–269.
(18) Barber, J. *Curr. Opin. Struct. Biol.* **2002**, *12*, 523–530.

(19) Diner, B. A.; Nixon, P. J.; Farchaus, J. W. *Curr. Opin. Struct. Biol.* **1991**, *1*, 546–554.
(20) Diner, B. A. *Biochim. Biophys. Acta* **2001**, *1503*, 147–163.
(21) Debus, R. J. *Biochim. Biophys. Acta* **2001**, *1503*, 164–186.

Table 1. Protein Subunits Assigned in the Crystal Structure of PSII Isolated from *T. elongates*[7] Giving Their Gene and Protein Nomenclatures, Molecular Masses, Numbers of Amino Acids (aa), and Numbers of Transmembrane α Helices[a]

gene	subunit	mass, kDa (aa)	no. of transmembrane α helices
PsbA	D1	39.737 (360)	5
PsbB	CP47	56.604 (510)	6
PsbC	CP43	51.620 (473)	6
PsbD	D2	39.361 (352)	5
PsbE	α-cyt b559	9.442 (83)	1
PsbF	β-cyt b559	5.065 (45)	1
PsbH	H protein	7.354 (66)	1
PsbI	I protein	4.405 (38)	1
PsbJ	J protein	4.150 (40)	1
PsbK	K protein	5.026 (46)	1
PsbL	L protein	4.297 (37)	1
PsbM	M protein	3.981 (36)	1
PsbYcf12*	Ycf12 protein	5.037 (46)	1
PsbO	O protein	20.608 (272)	0
PsbT	T protein	3.875 (32)	1
PsbU	U protein	15.018 (134)	0
PsbV	V protein	15.040 (137)	0
PsbX	X protein	5.232 (50)	1
PsbZ	Z protein	6.764 (62)	2

[a] Tentative assignment to PsbN by Ferreira et al.[7] but likely to be the product of the PsbYcf12 gene.[22]

The crystal structures of PSII[5–8] confirmed that the transmembrane helices of the D1 and D2 proteins are arranged in a way almost identical to those of the L and M subunits of the purple bacterial RC.[23,24] The six transmembrane helices of CP43 and CP47 are, in both proteins, arranged in three pairs around a pseudo-three-fold axis as first shown by electron crystallography.[15,16] These two Chl-binding proteins are located on each side of the D1 and D2 subunits in such a way that their transmembrane helices are related by the same pseudo-two-fold axis that relates the five transmembrane helices of the D1/D2 heterodimer, an organization very similar to that of the RC core proteins of PSI.[15,25,26]

3.2. Cofactors. The Ferreira et al. structural analysis[7] identified per monomer 36 Chls and tentatively assigned 7 carotenoids, assumed to be *all-trans-β*-carotene (see Figure 2). It was concluded that CP43 and CP47 bound 14 and 16 Chls, respectively, and in the majority of cases, these light-harvesting Chls were ligated by either α or β linkages to conserved histidine side chains and related by the same pseudo-two-fold symmetry axis that relates their transmembrane helices.[27] The Chls were arranged in layers toward the lumenal and stromal surfaces, with one Chl in each case located midway between the layers. Remarkably, the majority of the Chls bound to CP43 and CP47 have counterparts bound in the N-terminal domains of the *psa*A and *psa*B RC proteins of PSI.[27] A more recently determined crystal structure of cyanobacterial PSII at 3 Å resolution has assigned 11 *all-trans-β*-carotenes and concluded that CP43 binds 13 Chls rather than 14.[8]

As mentioned earlier, the D1 and D2 proteins contain the cofactors that bring about charge separation, leading to the oxidation of water and reduction of the terminal electron/proton acceptor, PQ. Together they bind six Chl a molecules, two Pheo molecules, two PQs, at least one β-carotene on the D2 side of the RC (Loll et al.[8] have recently assigned an additional nonsymmetrically related β-carotene on the D1 side), and a nonheme Fe. The Ferreira et al. crystal structure,[7] and also those reported by others,[5,6,8] clearly showed that these cofactors are also arranged around the pseudo-two-fold axis, which relates the transmembrane helices of D1, D2, CP43, and CP47 (see Figure 2). The axis passes through the nonheme Fe and through the middle of a cluster of four Chl a molecules called P_{D1}, P_{D2}, Chl_{D1}, and Chl_{D2}, as shown in Figure 2, where the suffix denotes binding to the D1 and D2 proteins. Similarly, the two Pheos are referred to as $Pheo_{D1}$ and $Pheo_{D2}$. The Q_A and Q_B PQs are positioned equally on each side of the nonheme Fe and are bound to the sites located within the D2 and D1 proteins, respectively. The remaining two Chls (Chl_{ZD1} and Chl_{ZD2}) are also symmetrically related, being ligated to histidines located in the B-transmembrane α helices of the D1 and D2 proteins.

Photons are captured by the light-harvesting pigments and transferred as excitation energy to the cluster of four Chl a molecules (P_{D1}, P_{D2}, Chl_{D1}, and Chl_{D2}). Although P_{D1} and P_{D2} are located close to each other, excitonic interaction between their tetrapyrolle head groups is weak and they do not form a "special pair", as found in other types of RCs.[26,28] Their monomeric character, therefore, makes them approximately isoenergetic with each other and also with the two accessory Chls, Chl_{D1} and Chl_{D2}. Therefore, it seems that excitation energy arriving at this cluster is delocalized over all four Chls to form the P* state.[29] The initial electron transfer probably occurs from Chl_{D1} because it is the closest to $Pheo_{D1}$ to form the charge-transfer state $Chl_{D1}^{•+}$-$Pheo_{D1}^{•-}$.[30,31] This radical pair state is short-lived, with migration of the "hole" to P_{D1} to form $P_{D1}^{•+}Pheo^{•-}$, where $P_{D1}^{•+}$ corresponds to the long-lived P radical cation. The electron on $Pheo_{D1}$ then proceeds down the thermodynamic gradient to the terminal PQ electron acceptor bound to the Q_B site within the D1 protein. As mentioned earlier, this electron transfer occurs in a few milliseconds and is aided by a fast intermediate electron transfer from $Pheo^{•-}$ to the PQ bound in the Q_A site of the D2 protein. On receiving two electrons, the PQ is protonated to plastoquinol PQH_2 and leaves the PSII complex by detachment from the Q_B site. The reduction of $P_{D1}^{•+}$ is brought about by removal of an electron from the Mn_4Ca cluster, thus driving a Mn ion into a higher valency state. This electron-transfer process is aided by a redox-active tyrosine, which is the D1 protein

(22) Kashino, Y.; Takahashi, T.; Inoue-Kashino, N.; Ban, A.; Yohei Ikeda, Y.; Satoh, K.; Sugiura, M. *Biochim. Biophys. Acta* **2007**, *1767*, 1269–1275.
(23) Barber, J. *Trends Biochem. Sci.* **1987**, *12*, 321–326.
(24) Michel, H.; Deisenhofer, J. *Biochemistry* **1988**, *27*, 1–7.
(25) Schubert, W. D.; Klukas, O.; Saenger, W.; Witt, H. T.; Fromme, P.; Krauss, N. *J. Mol. Biol.* **1998**, *280*, 297–314.
(26) Jordan, P.; Fromme, P.; Witt, H. T.; Klukas, O.; Saenger, W.; Kraus, N. *Nature* **2001**, *411*, 909–916.
(27) Murray, J. W.; Duncan, J.; Barber, J. *Trends Plant Sci.* **2006**, *11*, 152–158.
(28) Deisenhofer, J.; Epp, O.; Miki, K.; Huber, R.; Michel, H. *Nature* **1985**, *318*, 618–624.
(29) Durrant, J. R.; Klug, D. R.; Kwa, S. L. S.; van Grondelle, R. V.; Porter, G.; Klug, D. R. *Proc. Natl. Acad. Sci. U.S.A.* **1995**, *92*, 4798–4802.
(30) Prokhorenko, V. I.; Holzwarth, A. R. *J. Phys. Chem.* **2000**, *104*, 11563–11578.
(31) Dekker, J. P.; van Grondelle, R. *Photosynth. Res.* **2000**, *63*, 195–208.

residue Tyr161, denoted as Try_Z in Figure 2. This tyrosine has a symmetrically related counterpart within the D2 protein, Tyr_D (see Figure 2), which can also be oxidized by $P_{D1}^{\cdot+}$ but is not directly involved in the water-splitting reaction. It may, however, help to direct primary charge separation to the D1 side of the RC by electrostatic biasing.[32] This symmetrical relationship ends here because the Mn_4Ca cluster is only located on the D1 side while β-carotene and the nearby heme of Cyt b559 are located on the D2 side. Therefore, the D1 side of the RC functions directly in energy conversion and water splitting, while the D2 side is, in part, involved in protection against photoinduced damage.

Despite the symmetric arrangement of cofactors on the reducing side, electron transport from P_{D1} to terminal PQ involves only $Pheo_{D1}$ while the other possible route via $Pheo_{D2}$ does not occur, a situation that is also found for electron transfer in the RCs of purple photosynthetic bacteria.[28,33] In fact, the arrangement of the cofactors on the reducing side of PSII is essentially identical to that of their bacterial counterparts, with the only clear exceptions being that one of the ligands for the nonheme Fe of PSII is a bicarbonate ion and not a glutamate as in bacteria and that the Q_B site is a little larger and in closer contact with the stromal surface than in the bacterial RC. That bicarbonate probably provides a bidentate ligand for the nonheme Fe has been known for some time,[34,35] although the reason for this is unclear. Its removal slows Q_A to Q_B electron transfer and therefore may represent a feedback mechanism from CO_2 fixation to regulate PSII activity.

4. Structure of the Catalytic Site of the OEC

4.1. Based on X-ray Crystallography. It is on the oxidizing side where the water-splitting chemistry occurs that makes PSII distinctly different from its anoxygenic bacterial cousin. Indeed, it has been the holy grail of photosynthesis research to reveal the organization of the Mn_4Ca cluster and describe its protein environment with the view to elucidate fully the molecular mechanisms of the water-splitting reaction and dioxygen formation. From their X-ray diffraction analysis, Zouni et al.[5] showed that the electron density due to the Mn_4 cluster was "pear-shaped" when contoured at 5σ having dimensions of 6.8 Å × 4.9 Å × 3.3 Å, with the long axis approximately parallel to a surface α helix joining the lumenal ends of transmembrane helices C and D of the D1 protein and tilted at about 23° to the membrane plane. Because of the low resolution of the model, including the absence of side chains, the assignment of Mn ions within the density was rather arbitrary. A Mn ion was positioned in the three bulges of the "pear-shaped" density to form an isosceles triangle, with a fourth Mn ion placed above the center of the triangle. The distance between the Mn ions was about 3 Å and therefore approximately consistent with

extended edge X-ray absorption fine structure (EXAFS) analyses.[36] However, these workers did not propose a position for Ca^{2+} or attempt to model bridging ligands.

The 3 + 1 organization of the four Mn ions modeled by Zouni et al.[5] gave support to the arrangement suggested by Peloquin and colleagues[37,38] and also by Hasegawa et al.,[39] based on electron paramagnetic resonance (EPR) studies and was also a feature of the crystallographic model of the Mn_4 cluster published by Kamiya and Shen 2 years later.[6] However, in this later work, the four Mn ions were positioned approximately in the same plane, whereas Zouni et al.[5] had placed the central Mn ion protruding toward the lumenal surface.

It was the crystal structure of Ferreira et al.[7] that provided the first detailed structural information about the water-splitting catalytic site that had eluded us until then. The electron density map coupled with anomalous diffraction measured at specific wavelengths (1.95 Å for Mn and 2.25 Å for Ca^{2+}) indicated that the catalytic center did indeed contain four Mn ions and one Ca ion and that the Ca^{2+} and three Mn ions seem to form a cubane-like structure, where the four metals were proposed to be linked by oxo bonds. Ferreira et al. also proposed that the fourth Mn ion is linked to the Mn_3CaO_4 cubane by one of the O atoms of the cubane (see Figure 3).

The distances between the metal ions were modeled to be consistent with the type of linkage (di-μ-oxo or mono-μ-oxo) suggested from EXAFS studies conducted by Klein, Yachandra, Sauer, and colleagues at the University of California at Berkeley[36,40–44] (within the cubane, 2.7 and 3.4 Å for Mn–Mn and Mn–Ca, respectively, and 3.3 Å for the fourth Mn (Mn4 in Figure 3) to Mn within the cubane). These precise positioning and distances were tentative, being restricted by the resolution of the X-ray data and by the fact that some modifications may occur during exposure to X-rays. The crystals used for the analysis were grown from dark-treated PSII RC cores, which would reside in the S_1 state. However, the generation of free electrons in the crystal by the X-ray beam could reduce some of the high-valency Mn (thought to be Mn^{III} and Mn^{IV} in the S_1 state) to Mn^{II}.[45–47] In addition to the electron density assigned to the metal

(32) Faller, P.; et al. *Proc. Natl. Acad. Sci. U.S.A.* **2001**, *98*, 14368–14373.

(33) Feher, G.; Allen, J. P.; Okamura, M. Y.; Rees, D. C. *Nature* **1989**, *339*, 111–116.

(34) Hienerwadel, R.; Berthomieu, C. *Biochemistry* **1995**, *34*, 16288–16297.

(35) Govindjee; van Rensen, J. J. S. In *The Photosynthetic Reaction Center*; Deisenhofer, J. B., Norris, J., Eds.; Academic Press: San Diego, 1993; pp 357–389.

(36) Yachandra, V. K.; Sauer, K.; Klein, M. P. *Chem. Rev.* **1996**, *96*, 2927–2950.

(37) Peloquin, J. M.; Campbell, K. A.; Randall, D. W.; Evanchik, M. A.; Pecoraro, V. L.; Armstrong, W. H.; Britt, R. D. *J. Am. Chem. Soc.* **1998**, *120*, 6840–6841.

(38) Peloquin, J. M.; Britt, R. D. *Biochim. Biophys. Acta* **2001**, *1503*, 96–111.

(39) Hasegawa, K.; Ono, T. A.; Inoue, Y.; Kusunoki, M. *Chem. Phys. Lett.* **1999**, *300*, 9–19.

(40) Cinco, R. M.; McFarlane, Holman, K. L.; Robblee, J. H.; Yano, J.; Pizarro, S. A.; Bellacchio, E.; Sauer, K.; Yachandra, V. K. *Biochemistry* **2002**, *41*, 12928–12933.

(41) DeRose, V. J.; Mukerji, I.; Latimer, M. J.; Yachandra, V. K.; Sauer, K.; Klein, M. P. *J. Am. Chem. Soc.* **1994**, *116*, 5239–5249.

(42) Robblee, J. H.; Cinco, R. M.; Yachandra, V. K. *Biochim. Biophys. Acta* **2001**, *1503*, 7–23.

(43) Robblee, J. H.; Messinger, J.; Cinco, R. M.; McFarlane, K. L.; Fernandez, C.; Pizarro, S. A.; Sauer, K.; Yachandra, V. K. *J. Am. Chem. Soc.* **2002**, *124*, 7459–7471.

(44) Yachandra, V. K. *Philos. Trans. R. Soc. London* **2002**, *B357*, 1347–1358.

(45) Dau, H.; Liebisch, P.; Haumann, M. *Phys. Chem. Chem. Phys.* **2004**, *6*, 4781–4792.
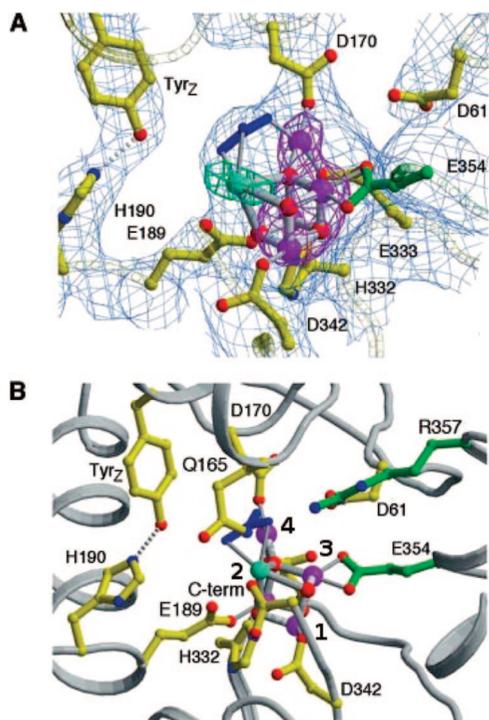
Figure 3. Structure of the water-splitting site from Ferreira et al.:[7] view of the metal cluster (A) with side-chain ligands and (B) with possible catalytically important side-chain residues. Mn ions, Ca^{2+}, and O atoms are shown in magenta, cyan, and red, respectively. One unidentified nonprotein ligand to the OEC and modeled as carbonate is colored in blue. The protein main chain is depicted in light gray, while the side-chain bonds and C atoms follow the coloring of the protein subunits (D1, yellow; CP43, green). In part A, the σ_A-weighted $2|F_o| - |F_c|$ density is shown as a light-blue wire mesh contoured at 1.5σ. Anomalous difference Fourier maps at 1.89340 Å (Mn edge, contoured at 10σ) and 2.25430 Å (highlights Ca^{2+}, contoured at 7σ) wavelengths are shown in magenta and blue-green, respectively.

cluster and surrounding amino acids, density was tentatively assigned to a carbonate ion bridging between the Mn outside the cubane (Mn4) and Ca^{2+}, as shown in Figure 3. It remains to be seen whether such an assignment is correct, but there are several experimental observations suggesting that this anion is a cofactor for the water-splitting reaction of PSII.[48–51]

Despite the uncertainty of the valency states and precise organization of the cluster, Ferreira et al.[7] identified six amino acid ligands for the Mn_4Ca^+ cluster, five from the D1 protein (Asp170, Glu189, His332, Glu333, and Glu342) and surprisingly one from the large extrinsic loop of CP43 (Glu354) (see Figure 3). Three of the D1 residues are located in its C-terminal domain, while the other two (Glu189 and Asp170) are positioned in a lumenal loop joining transmembrane helices C and D. All of them had been predicted by site-

directed mutagenesis to be possible ligands to the Mn_4Ca cluster or near to it.[19–21,52] In contrast, the CP43 ligand (Glu354) had not been predicted to be an intimate part of the water-splitting site although mutagenesis of this residue had hinted at its involvement in water oxidation catalysis.[53] This glutamate forms a part of a fully conserved region of CP43, which Ferreira et al.[7] showed to be a 3_{10} helix. Also close to the metal cluster are other side chains that are, or are likely to be, very important to its catalytic activity (Figure 3). In particular, the redox-active tyrosine D1 Tyr161 (Tyr_Z) is about 6.5 Å from Mn4 and 5 Å from Ca^{2+} of the cluster, sufficient to facilitate rapid electron extraction. The phenolic group of Tyr_Z is also in a hydrogen-bonding distance to D1 His190, which would allow it to be deprotonated and form a neutral radical ($Tyr_Z^\bullet$) when oxidized by $P_{D1}^{\bullet+}$, in line with EPR studies of Babcock and others.[54–57] Nearby, CP43 Arg357 (also a part of the 3_{10} helix) and D1 Glu167 probably play essential roles in forming hydrogen-bonding networks necessary to deprotonate the substrate water molecules during catalysis.[58]

Two residues, D1 Asp61 and D2 Lys317, form the beginning of a polar channel that leads away from the catalytic site to the lumenal surface. This polar channel is about 35 Å long and involves residues within the PsbO extrinsic protein. A Ca^{2+} ion is bound at its lumenal exit point.[59] This channel is probably the exit route for protons derived from water splitting, but it could also be the route for substrate water molecules to reach the catalytic site. The Ca^{2+} ion at the lumenal end may help to order water molecules, thus facilitating protons to leave and water to enter the channel. Two other channels leading to and from the OEC have also been identified,[60] one of which is relatively polar and could also be involved in water or proton transfer while the other is sufficiently hydrophobic that it could represent an exit pathway for the rapid removal of oxygen from the catalytic site. These three channels are detailed in Figure 4. (Very recently, Ho and Styring[93] have also proposed several channels leading from the OEC to the lumenal surface that could transport protons, water, or oxygen.)

The crystal structure of Ferreira et al.[7] has stimulated others[61,62] to develop theoretical models for the catalytic site where the Mn_4Ca cluster is completely ligated by amino acid

(46) Grabolle, M.; Haumann, M.; Muller, C.; Liebisch, P.; Dau, H. *J. Biol. Chem.* **2006**, *281*, 4580–4588.
(47) Yano, J.; et al. *Proc. Natl. Acad. Sci. U.S.A.* **2005**, *102*, 12047–12052.
(48) Allakhverdiev, S. I.; Yruela, I.; Picorel, R.; Klimov, V. V. *Proc. Natl. Acad. Sci. U.S.A.* **1997**, *94*, 5050–5054.
(49) Baranov, S. V.; Ananyev, G. M.; Klimov, V. V.; Dismukes, G. C. *Biochemistry* **2000**, *39*, 6060–6065.
(50) Klimov, V. V.; Baranov, S. V. *Biochim. Biophys. Acta* **2001**, *1503*, 187–196.
(51) van Rensen, J. J. S.; Klimov, V. V. *Photosystem II. The light driven water: plastoquinone oxidoreductase*; Satoh, K., Wydrzynski, T. J., Eds.; Springer: Dordrecht, The Netherlands, 2005; pp 329–346.

(52) Chu, H.-A.; Hillier, W.; Debus, R. J. *Biochemistry* **2004**, *43*, 3152–3166.
(53) Rosenberg, C.; Christian, J.; Bricker, T. M.; Putnam-Evans, C. *Biochemistry* **1999**, *38*, 15994–16000.
(54) Barry, B. A.; Babcock, G. T. *Proc. Natl. Acad. Sci. U.S.A.* **1987**, *84*, 7099–7103.
(55) Hoganson, C. W.; Babcock, G. T. *Science* **1997**, *27*, 1953–1956.
(56) Tommos, C.; Babcock, G. T. *Biochim. Biophys. Acta* **2000**, *1458*, 199–219.
(57) Babcock, G. T.; Espe, M.; Hogansson, C.; Lydakis-Simantiris, N.; McCracken, J.; Shi, W.; Styring, S.; Tommos, C.; Warncke, K. *Acta Chem. Scand.* **1997**, *51*, 533–540.
(58) McEvoy, J. P.; Gascon, J. A.; Batista, V. S.; Brudvig, G. W. *Photochem. Photobiol. Sci.* **2005**, *4*, 940–949.
(59) Murray, J. W.; Barber, J. *Biochemistry* **2006**, *45*, 4128–4130.
(60) Murray, J. W.; Barber, J. *J. Struct. Biol.* **2007**, *159*, 228–237.
(61) Sproviero, E. M.; Gascon, J. A.; McEvoy, J. P.; Brudvig, G. W.; Batista, V. S. *J. Chem. Theory Comput.* **2006**, *2*, 1119–1134.
(62) Sproviero, E. M.; Gascon, J. A.; McEvoy, J. P.; Brudvig, G. W.; Batista, V. S. *Curr. Opin. Struct. Biol.* **2007**, *17*, 173–180.
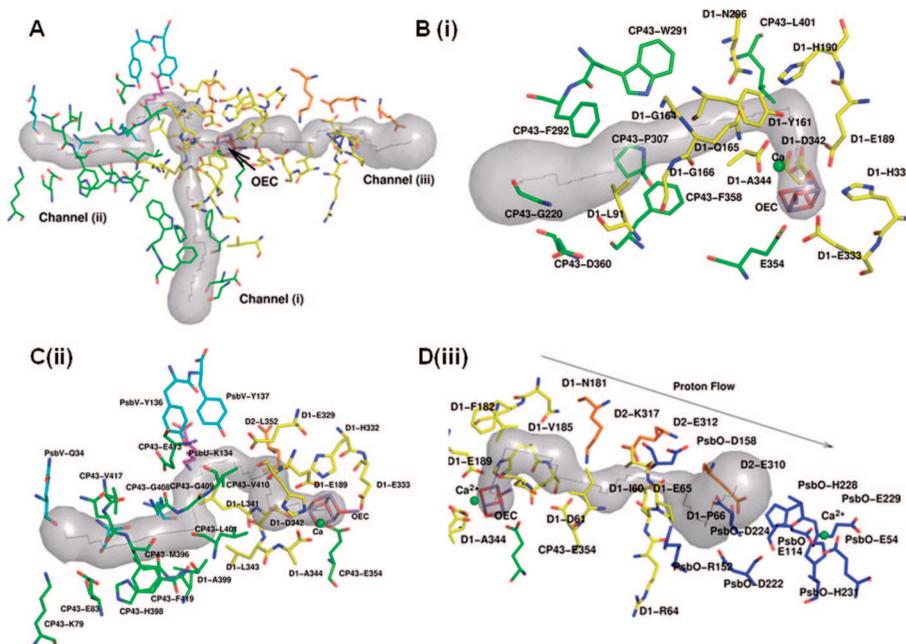
Figure 4. Identification of three channels leading from the OEC to the lumenal side of PSII.[60] (A) All three channels identified by analyses using the program *CAVER*.[91] (B) Details of channel i suggested to be a route for oxygen to diffuse from the OEC. (C) Details of channel ii, which could act as a proton/water channel for the OEC. (D) Details of channel iii, which has been identified previously as a likely proton/water channel for the OEC.[7,92] The Ca^{2+} binding site on the PsbO protein[59] is also shown. Amino acid residues within 4 Å of the center of the pathway are shown in a stick representation and are color-coded to their respective proteins as follows: D1, yellow; CP43, green; D2, orange; PsbV, cyan; PsbU, magenta. Modified from Murray and Barber.[60]

residues, water molecules, hydroxides, and chloride. State-of-the-art density function theory (DFT) involving quantum mechanical molecular mechanics (QM/MM) hybrid methods was used to investigate the intrinsic properties of the metal cluster and predict the perturbational influence of the protein environment on the structural and electronic properties of the catalytic center. Overall, the calculations broadly supported the structural model for the Mn_4Ca cluster derived from the crystallographic analysis of Ferreira et al.[7] and, moreover, concluded that when it is completely ligated with water, OH^-, Cl^-, and amino acids, it is a stable molecular structure even when the surrounding protein environment is removed. The synthesis of a mixed Mn/Ca complex[63] also suggested that the organization of the Mn_4Ca^{2+} cluster proposed by Ferreira et al.[7] was chemically feasible despite there being no known similar structure in biology.

Toward the end of 2005, a new crystal structure of PSII isolated from *T. elongatus* was published by Loll et al.,[8] continuing on from an earlier study.[64] The resolution of the structure was reported to be 3.0 Å. For the most part, this new model confirmed the subunit and amino acid assignment and side-chain positioning reported by Ferreira et al.,[7] with minor differences within the limitation imposed by the intermediate resolution of the X-ray diffraction data. Nevertheless, the improved electron-density map allowed Loll et al. to correct and extend the original assignment of β-carotene molecules by Ferreira et al.[7] and to locate several bound lipid molecules. As in the earlier papers from this

group,[5] the pear-shaped electron density attributed to the metal cluster of the water-splitting site was interpreted as four Mn cations organized in a Y shape or 3 + 1 arrangement. Based on anomalous diffraction, the Ca^{2+} was placed in a position similar to that proposed by Ferreira et al.,[7] and recently confirmed by Kargul et al.,[65] whereas the positioning of three of the Mn ions was different from that suggested by Ferreira et al.[7] The fourth Mn ion was assigned to the narrow end of the pear-shaped density in a position slightly different from that of Ferreira et al.[7] or Zouni et al.[5] The Loll et al. model[8] of the metal cluster, like that of Ferreira et al.,[7] had distances between the metal ions that were in line with those derived from EXAFS measurements.[44] They assumed di-μ-oxo bridges of 2.7 Å between Mn1 and Mn2 and between Mn2 and Mn3, while Mn1–Mn3 and Mn3–Mn4 were modeled at 3.3 Å, as expected for mono-μ-oxo bridging. The electron density surrounding the Mn_4Ca cluster was assigned to the same amino acids first identified in the crystal structure of Ferreira et al.,[7] although there were differences in the precise locations in some cases. Within the errors of the two models, Loll et al. confirmed the Ferreira et al.[7] assignment of most of the key residues in the water-splitting site. The most striking difference was the position of D1 Asp170 and to a lesser extent D1 Asp342 and D1 Ala344. With these differences, coupled with the different positioning of the Mn ions, Loll et al.[8] proposed an amino acid coordination arrangement modified from that provided earlier by Ferreira et al.[7] However, Loll et al.[8] emphasized that their model for the OEC was tentative, in part because of the low

(63) Misra, A.; Wernsdorfer, W.; Abboud, K. A.; Christou, G. *Chem. Commun. (Cambridge, U.K.)* **2005**, 54–56.

(64) Biesiadka, J.; Loll, B.; Kern, J.; Irrgang, K. D.; Zouni, A. *Phys. Chem. Chem. Phys.* **2004**, *6*, 4733–4736.

(65) Kargul, J.; Maghlaoui, K.; Murray, J. W.; Deak, Z.; Boussac, A.; Rutherford, A. W.; Vass, I.; Barber, J. *Biochim. Biophys. Acta* **2006**, *1767*, 404–413.

resolution of the electron-density map and in part because of radiation damage. Working with the EXAFS group at Berkeley, and prior to the publication of the Loll et al. crystal structure,[8] the same group had shown that doses of X-rays typical of those used for diffraction analyses caused the reduction of the Mn cluster and associated structural changes[47] and therefore questioned the validity of the structural models of the OEC derived from X-ray crystal-lography. This problem of radiation damage occurring at the Mn cluster had also been highlighted by Dau et al.[45] and investigated further by Grabolle et al.[46]

Despite the uncertainties of the Ferreira et al. and Loll et al. models regarding the Mn cluster, the concept of bidentate bridging ligands proposed in the latter is worthy of serious consideration given that this type of ligation is common in Mn-containing enzymes such as arginase,[66] *Escherichia coli* ribonucleotide reductase,[67] and others[68] as well as in Mn-containing model compounds.[69] The presence of bridging carboxylate ligands may explain mutational studies directed at the OEC, where the exchange of some of the proposed ligands with nonliganding side chains using mutagenesis does not disrupt the Mn_4Ca cluster or inhibit water oxidation.[20,21]

4.2. Models Based on Combining X-ray Crystallo-graphy and EXAFS Data. Recently, Barber and Murray[70,71] have considered some alternative interpretations of the structure of the OEC using currently available data from both X-ray crystallography and X-ray absorption spectroscopy. The modeling was based on the Mn-anomalous difference map of Ferreira et al.[7] and the recent EXAFS data of Yano et al.[72] and favored bidentate and bridging ligation where possible. The Mn-anomalous data of Ferreira et al.[7] seem to be the most reliable at present and are available via the PDB database. Although it is at a resolution of 3.8 Å, it has the advantage of not being biased to the model phases and at this resolution is probably not influenced significantly by any radiation modifications.

4.2.1. Modification of the Model of Ferreira et al[7]. The EXAFS determination of Mn–Mn distances by Yano et al.[72] was consistent with the earlier studies of Yachandra and colleagues,[36,44] which indicated that the Mn cluster of the OEC is composed of three Mn–di-μ-oxo–Mn bridges and only one mono-μ-oxo bridge. (There remains controversy in the literature regarding the numbers of Mn–mono-μ-oxo–Mn and Mn–di-μ-oxo–Mn bonds based on EXAFS measurements. For example, Dau and colleagues provide evidence for two, not three, Mn–di-μ-oxo–Mn bonds in the S_1 state.[45,89]) According to the original model of Ferreira et al.,[7] there were indeed three Mn–di-μ-oxo–Mn bonds but two mono-μ-oxo bridges due to the proposed linkage of Mn4

to the cubane via one of its O atoms. For this reason, Barber and Murray[70] considered an alternative interpretation by assuming that Mn4 is linked to the Mn_3CaO_4 cluster via one of the Mn ions of the cubane (Mn3). Maintaining the approximate agreed positioning of the Ca ion[7,8,65] requires a repositioning of the other three Mn ions in this modified model of Ferreira et al.[7] This repositioning of the Mn ions together with slight changes in the assignment of side-chain orientations resulted in the protein ligation pattern shown in Figure 5C, where it is compared with the original Ferreira model (Figure 5A). Parts B and D of Figure 5 show a schematic representation of the ligation pattern for the Ferreira et al. model[7] and its modified form, respectively. The coordination numbers for Mn are five or six, and according to the model shown in Figure 5C, this requirement is better satisfied by amino acid side chains than in the original Ferreira et al. model (Figure 5A,B) because of the introduction of bidentate and bridging ligation: six for Mn1, six for Mn2, six for Mn3, and four for Mn4. The overall positioning of the Mn ions in the modified model and the pattern of amino acid ligation are similar to those proposed by Loll et al.[8] (with some exceptions). However, the average orientations to the membrane normal of the three Mn–di-μ-oxo–Mn bonds (81°) and the Mn–mono-μ-oxo–Mn bond (47°) are not consistent with those recently derived from polarized EXAFS,[47,73] which indicates 40–60° and 90°, respectively.

Although the major difference between the new model derived by Barber and Murray[70,71] and that of Ferreira et al.[7] is the relocation of the Mn ions so as to accommodate only one Mn–mono-μ-oxo–Mn bond, the slight changes in the orientation of some side chains also make some differences to the original Ferreira et al. model: D1 Ala344 is now in a ligating distance to Mn2 as well as Ca^{2+}, and bridging ligands are also proposed between Mn1 and Mn2 (D1 Asp342), Mn2 and Mn3 (CP43 Glu354), and Mn3 and Mn4 (D1 Glu333).

4.2.2. EXAFS-Based Models. The cubane model proposed by Ferreira et al.[7] or its modified form considered by Barber and Murray[70,71] (Figure 5), or the Loll et al. model,[8] is not consistent with any of the four models recently proposed from polarized EXAFS spectroscopy as applied to single crystals.[72] The EXAFS analysis gives high-resolution information about the possible arrangement of the metal ions, but for a complete structure of the OEC, the EXAFS-derived models must be accommodated within the protein environment of the catalytic site. To do this, Yano et al.[72] combined the EXAFS models with the electron-density map of Loll et al.[8] More recently, Barber and Murray[71] reconsidered this fitting by using the Mn-anomalous diffraction difference map derived by Ferreira et al.[7] as a guide. They found that none of the recently proposed EXAFS models fitted comfortably

(66) Kanyo, Z. F.; Scolnick, L. R.; Ash, D. E.; Christianson, D. W. *Nature* **1996**, *383*, 554–557.

(67) Sommerhalter, M.; Saleh, L.; Bollinger, J. M., Jr.; Rosenzweig, A. C. *Acta Crystallogr., Sect. D: Biol. Crystallogr.* **2005**, *61*, 1649–1654.

(68) Dismukes, G. C. *Chem. Rev.* **1996**, *96*, 2909–2926.

(69) Christou, G. *Acc. Chem. Res.* **1989**, *22*, 328–335.

(70) Barber, J.; Murray, J. W. *Coord. Chem. Rev.* **2007**, in press.

(71) Barber, J.; Murray, J. W. *Philos. Trans. R. Soc. London* **2007**, in press.

(72) Yano, J.; Kern, J.; Sauer, K.; Latimer, M. J.; Pushkar, Y.; Biesiadka, J.; Loll, B.; Saenger, W.; Messinger, J.; Zouni, A.; Yachandra, V. K. *Science* **2006**, *314*, 821–825.

(73) Pushkar, Y.; Yano, J.; Glatzel, P.; Messinger, J.; Lewis, A.; Saure, K.; Bergmann, U.; Yachandra, V. K. *J. Biol. Chem.* **2007**, *282*, 7198–7208.

(87) Emsley, P.; Cowtan, K. *Acta Crystallogr., Sect. D: Biol. Crystallogr.* **2004**, *60*, 2126–2132.

(88) Miyashita, H.; Ikemoto, H.; Kurano, N.; Adachi, K.; Chihara, M.; Miyachi, S. *Nature (London)* **1996**, *383*, 402.
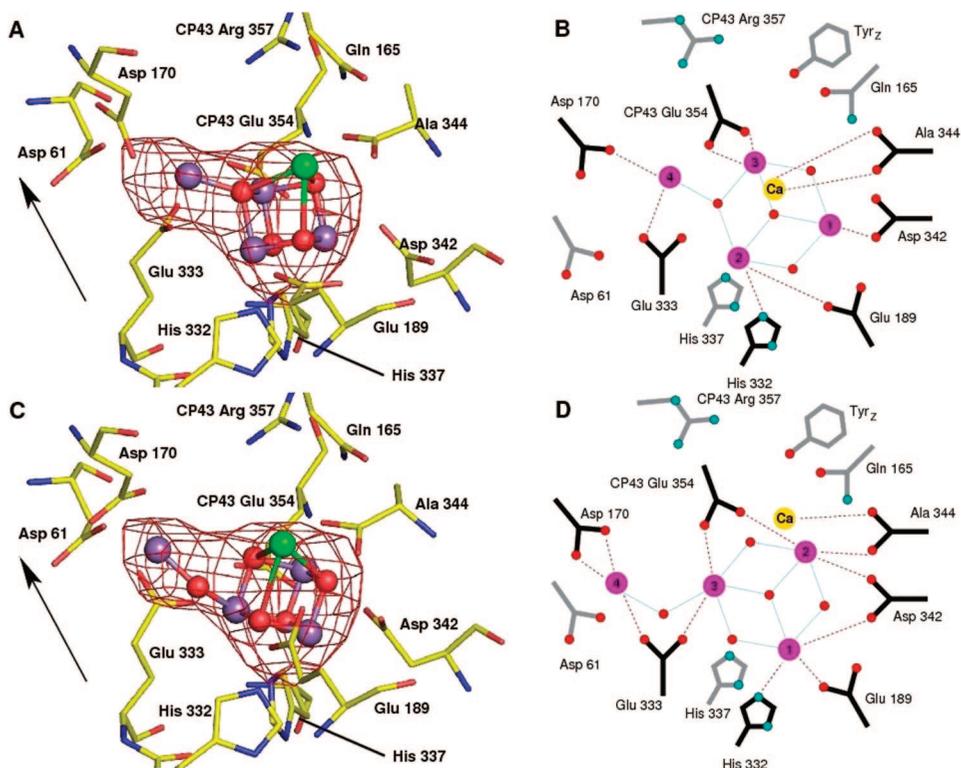
Figure 5. Two models of the catalytic site of the OEC based on X-ray crystallography. (A) The Mn$_4$Ca cluster as proposed by Ferreira et al.[7] positioned within the Mn-anomalous difference map of Ferreira et al.[7] with amino acid side chains. (B) Schematic representation of the amino acid ligation pattern for the model in part A with a distance of less than 2.8 Å shown by connecting lines. (C) Remodeling the OEC by Barber and Murray[70] using the native electron-density maps of Ferreira et al.[7] and Loll et al.[8] and the Mn-anomalous difference map of Ferreira et al.,[7] keeping the Mn$_3$CaO$_4$ cubane of Ferreira et al. but with Mn4 (dangler Mn) linked to it via a single 3.3 Å mono-μ-oxo bridge. (D) Schematic representation of the amino acid ligation pattern for the model in part C with a distance of less than 2.8 Å shown by connecting lines. The Mn-anomalous difference map is shown in red and contoured at 5σ. The arrow indicates the direction of the normal to the membrane plane. The fitting of the models for the metal cluster was performed by real-space refinement using the molecular graphics program *Coot*.[87]

into the Mn-anomalous diffraction map using the coordinates provided by Yano et al.[71] Using real-space refinement against the Mn-anomalous difference density to obtain a revised fitting and recognizing that there are discrepancies in the determination of the bond angles relative to the membrane normal, as emphasized by a comparison of Yano et al.[72] with Pushkar et al.[73] or by reference to earlier work,[74–76] they slightly adjusted the positioning of the four EXAFS models so as to improve their fit within the Mn-anomalous difference map (see Figure 6). These new fittings within the Mn-anomalous difference map gave orientations to the membrane normal of the Mn–di-μ-oxo–Mn bonds (2.7 and 2.8 Å) and the Mn–mono-μ-oxo–Mn bonds (3.3 Å), as shown in Table 2, where they are compared with those derived from the coordinates of Yano et al.[72] The differences are in most cases not large and probably within experimental error.

As shown in Figure 6, the repositioning of the four EXAFS models into the crystal structure reveals differences in possible amino acid ligation patterns. As for the modified Ferreira et al. model shown in Figure 5C, the orientations of the carboxylate side chains were optimized using the native electron-density maps of Ferreira et al.[7] and Loll et

al.[8] with the view of possibly forming bidentate and bridging ligands whenever possible. All of the amino acids identified as potential ligands by Ferreira et al.[7] remain close to the metals, but the precise arrangements are different. For EXAFS models II, IIa, and III, D1 Ala344 forms a bidentate ligand with MnD (Mn1) while D1 Asp342 forms a monodentate ligand with this Mn (Figure 6D,F,H). D1 His332 remains a ligand for all four EXAFS models except for model I, where it is a ligand for MnD (Mn1), while for the other models, it ligates MnC (Mn2). D1 Glu333 is a ligand for MnA (Mn4) in all cases but with bidentate bridging to MnB (Mn3) in models II, IIa, and III. In all cases D1 Asp170 provides a single carboxylate ligand to MnA (Mn4). Only with EXAFS models I and III does D1 Glu189 form an exclusive bidentate ligand to Ca^{2+}, while in the other two models, it forms a bidentate bridge between Ca^{2+} and MnC (Mn2). The final amino acid ligand originally identified by Ferreira et al.[7] is CP43 Glu354. This residue appears to be in a ligating distance to Mn in all four EXAFS models. In model I, it is bidentate to MnB (Mn3), while in model III, its carboxylate O atoms bridge between MnB (Mn3) and MnC (Mn2). In models II and IIa, CP43 Glu354 provides a single ligand to MnB (Mn3).

5. Conclusion

X-ray crystallography has provided detailed information about the structure of PSII. The location and arrangement

(74) George, G. N.; Prince, R. C.; Cramer, S. P. *Science* **1989**, *243*, 789–791.
(75) Dittmer, J.; Dau, H. *J. Phys. Chem.* **1998**, *B102*, 8196–8200.
(76) Schiller, H.; Dittmer, J.; Iuzzolino, L.; Dörner, W.; Meyer-Klaucke, W.; Sole, V. A.; Nolting, H.-F.; Dau, H. *Biochemistry* **1998**, *37*, 7340–7350.
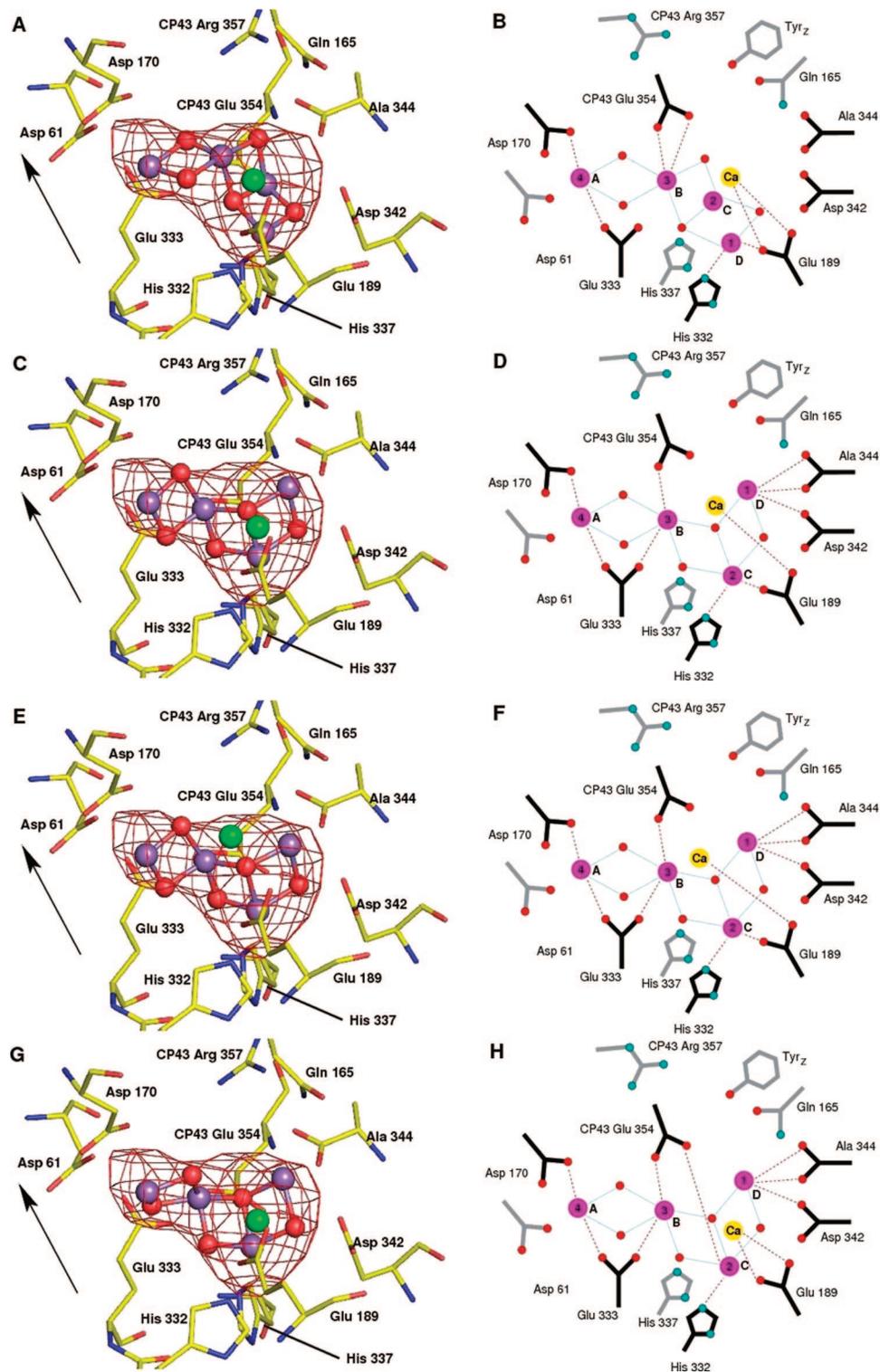
Figure 6. Refinement of the positioning of the EXAFS models (models I, II, IIa, and III) of Yano et al.[72] into the Mn-anomalous diffraction data of Ferreira et al.[7] by Barber and Murray.[71] Each EXAFS models were fitted by real-space refinement against the Mn-anomalous difference map of Ferreira et al.[7] using the molecular graphics program *Coot*.[87] The Mn-anomalous difference map is shown in red and contoured at 5σ. Parts A, C, E, and G are for EXAFS models I, II, IIa, and III, respectively, while parts B, D, F, and H are the schematic for each showing potential ligation patterns, where the lines are for distances of 2.8 Å or less. The arrows indicate the direction of the normal to the membrane plane.

of the majority of the protein subunits of PSII have been revealed including the organization of their transmembrane helices. The assignment of amino acids in these proteins as well as the organization of cofactors has been achieved. Although the resolution has to date been restricted to about 3.0 Å, the modeling of the majority of side-chain positions

is sufficiently good that there will be only slight modifications made as the resolution of the X-ray diffraction data improves. Similarly, this will be true for most of the cofactors. For this reason, the current description of the protein environments around the various cofactors involved in energy transfer and charge separation is reliable. The only major

Table 2. Calculated Bond Angles (deg) Relative to the Membrane Normal for Various Models of the Mn₄Ca Cluster of the OEC[a]

structure	mono-μ	mean di-μ	mean 3.4 Å (or nearer Ca²⁺ distance)	2.8 Å distance angle	mean 2.7 Å distance angle	rotation angle (from Yano to a real-space fit)
1S5L	58/37 (2 vals)	72	39			NA
2AXT	47/84 (2 vals)	74	31			NA
mono-μ-cubane	47	81	29			NA
model I	34, 66	61, 58	61, 32	85, 67	49, 54	34
model II	81, 87	48, 55	46, 33	60, 65	42, 50	27
model IIa	86, 89	50, 55	37, 32	57, 60	46, 52	36
model III	80, 83	49, 52	43, 36	63, 65	41, 46	24

[a] PDB coordinates 1S5L and 2AXT are for Ferreira et al.[7] and Loll et al.,[8] respectively. Mono-μ-cubane is the modified form of the Ferreira et al. model shown in parts C and D of Figure 5 from Barber and Murray.[70,71] Models I, II, IIa, and III are structures of the OEC modeled by Barber and Murray[71] based on the EXAFS-derived models of Yano et al.[72] and Mn-anomalous density of Ferreira et al.[7] for these four models. The first bond angle values are calculated from the original orientations and the second for the modified versions. The last column is the angle of real-space rotation compared with the original of Yano et al.[72] The table is taken from Barber and Murray.[71]

uncertainties are the precise structure of the OEC. The structural data currently available provide a number of alternative models for the metal–protein arrangements within this catalytic center. Improvement in the quality of X-ray diffraction data, collected in such a way as to reduce radiation damage, will be paramount for identifying which of the various models is the most reliable. Moreover, the resolution of X-ray diffraction data must be such to clearly assign water molecules with the view to identify those that act as the substrate during the catalytic cycle. Despite these challenges, the present models are consistent with the view that the "catalytic surface" of the metal cluster involves Mn4 and Ca²⁺, as first suggested by Ferreira et al.[7] and discussed in related publications.[77–79] These two ions are positioned toward a cavity containing various side chains that aid electron and proton removal, including D1 Tyr161 (Yz), D1 His189, D1 Gln165, D1 Asp61, and CP43 Arg357. In all cases, the distance between Mn4 and Ca²⁺ is about 4 Å, which is consistent with a mechanism whereby a substrate water within the coordination sphere of Ca²⁺ could act as a nucleophile for a highly electrophilic oxo generated by deprotonation of the second substrate water molecule and coordinated to a high valency state of Mn4 (possibly Mnⱽ). This mechanism has been championed particularly by Pecoraro,[80] Brudvig,[81,82] Messinger,[83,84] and their colleagues. An alternative mechanism preferred by Siegbahn,[85,86] which is also consistent with the geometry of the OEC models, involves an oxyl radical associated with Mn4 (possibly Mnⁱⱽ) attacking an oxo bridge between Mn4 and Ca²⁺.

Ultimately, the challenge of understanding precisely how photosynthetic organisms use sunlight to split water and make oxygen will require the successful coupling of X-ray diffraction data with information derived from EXAFS, Fourier transform IR (FTIR), EPR spectroscopy, and other techniques, including the application of DFT and QM/MM analyses.

(77) Barber, J.; Ferreira, K. N.; Maghlaoui, K.; Iwata, S. *Phys. Chem. Chem. Phys.* **2004**, *6*, 4737–4742.
(78) Barber, J.; Iwata, S. *Photosystem II. The light driven water: plastoquinone oxidoreductase*; Satoh, K., Wydrzynski, T. J., Eds.; Springer: Dordrecht, The Netherlands, 2005; pp 469–489.
(79) Barber, J. *Biochem. Soc. Trans.* **2006**, *34*, 619–631.
(80) Pecoraro, V. L.; Baldwin, M. J.; Caudle, M. T.; Hsieh, W.-Y.; Law, N. A. *Pure Appl. Chem.* **1998**, *70*, 925–929.
(81) McEvoy, J. P.; Brudvig, G. W. *Phys. Chem. Chem. Phys.* **2004**, *6*, 4754–4763.
(82) McEvoy, J. P.; Brudvig, G. W. *Chem. Rev.* **2006**, *106*, 4455–4483.
(83) Messinger, J.; Badger, M.; Wydrzynski, T. *Proc. Natl. Acad. Sci.* **1995**, *92*, 3209–3213.
(84) Messinger, J. *Phys. Chem. Chem. Phys.* **2004**, *6*, 4764–4771.

(85) Siegbahn, P. E. M.; Lundberg, M. *Photochem. Photobiol. Sci.* **2005**, *4*, 1035–1043.
(86) Siegbahn, P. E. M. *Chem.—Eur. J.* **2006**, *12*, 9217–9237.
(89) Haumann, M.; Muller, C.; Liebisch, P.; Iuzzolino, L.; Dittmer, J.; Grabolle, M.; Neisius, T.; Meyer-Klaucke, W.; Dau, H. *Biochemistry* **2005**, *44*, 1894–1908.
(90) De Las Rivas, J.; Barber, J. *Photosynth. Res.* **2004**, *81*, 329–343.
(91) Petřek, M.; Otyepka, M.; Banas, P.; Kosǐnová, P.; Koca, P.; Damborský, J. *BMC Bioinf.* **2006**, *7*, 316–324.
(92) Ishikita, H.; Saenger, W.; Loll, B.; Biesiadka, J.; Knapp, E.-W. *Biochemistry* **2006**, *45*, 2063–2071.
(93) Ho, F. M.; Styring, S. *Biochim. Biophys. Acta* **2007**, in press.